A NEW MECHANISM FOR RADIAL MIGRATION IN GALACTIC DISKS: SPIRAL-BAR RESONANCE OVERLAP

I. Minchev, Benoit Famaey

Draft version November 2, 2018
Preprint typeset using LaTeX style emulateapj v. 11/26/04

A NEW MECHANISM FOR RADIAL MIGRATION IN GALACTIC DISKS: SPIRAL-BAR RESONANCE OVERLAP

I. Minchev[1] & B. Famaey[1]

Draft version November 2, 2018

ABSTRACT

While it has long been known that a large number of short-lived transient spirals can cause stellar migration, here we report that another mechanism is also effective at mixing disks of barred galaxies. The resonance overlap of the bar and spiral structure induces a nonlinear response leading to a strong redistribution of angular momentum in the disk. We find that, depending on the amplitudes of the perturbers, the changes in angular momentum, ΔL, could occur up to an order of magnitude faster than in the case of recurrent spirals. The signature of this mechanism is a bimodality in ΔL with maxima near the bar's corotation and its outer Lindblad resonance; this is independent of the properties of the spiral structure. For parameters consistent with the Milky Way the disk mixes in about 3 Gyr and the stellar velocity dispersion increases with time in a manner roughly consistent with observations. This new mechanism could account for both the observed age-velocity relation and the absence of age-metallicity relation in the solar neighborhood. Spiral-bar interaction could also explain observations showing that strongly barred galaxies have weaker metallicity gradients than weakly barred or non-barred galaxies.

Subject headings: ISM: abundances — Galaxy: abundances — galaxies: ISM — Galaxy: evolution — galaxies: kinematics and dynamics — galaxies: structure

1. INTRODUCTION

The metallicity of the interstellar medium (ISM) in a galaxy is expected to increase with time due to the progressive enrichment through stellar feedback. Consequently, one would expect that younger stars formed at the same galactic radius would have higher metallicities. In addition, the ISM metallicity has been well established to decrease with increasing galactic radius, r, due to a more efficient star formation and enrichment of the ISM in the central regions of galaxies (Wilson and Rood 1994; Daflon and Cunha 2004). This in turn would result in coeval stars being progressively more metal-poor as r increases.

However, the metallicities of stars in the solar neighborhood (SN) have been observed to lack the expected correlation with age (Edvardsson et al. 1993; Haywood 2008). Re-examining the age-metallicity distribution of the Geneva-Copenhagen survey (Nordström et al. 2004), Haywood (2008) found that the data are only consistent with the age-metallicity relation (AMR) for stars younger than 3 Gyr. For other samples the width of the metallicity distribution was found to be larger than what could be accounted for by measurement errors and/or inhomogeneous ISM. Because of the age-velocity relation (AVR), where older stellar samples are observed to have higher velocity dispersion than younger ones (e.g. Holmberg et al. 2009), stars from the inner and outer Milky Way (MW) disk can enter the SN and thus blur the expected AMR. However, this can only account for about 50 % of the observed scatter (Nordström et al. 2004).

A possible explanation for this discrepancy is the radial migration of stars from their birth guiding radii (Haywood 2008; Schönrich and Binney 2009). Indeed, there is now considerable evidence that the non-axisymmetry of the Galactic potential can cause significant perturbations in the motion of both stars and gas: observational evidence for this comes from (i) the observed non-circular motions of gas flows in the inner MW (Bissantz et al. 2003), (ii) the large non-axisymmetric motions of star-forming regions (Xu et al. 2006), (iii) the moving groups in the SN (Dehnen 1998) containing stars of very different ages (Famaey et al. 2005; Antoja et al. 2008), suggesting that their clumping in velocity space is most likely not due to irregular star formation, but rather to dynamical perturbations from the bar (Dehnen 2000; Minchev et al. 2010a) and/or the spirals (e.g., Quillen and Minchev 2005, Antoja et al. 2009), or an orbiting satellite galaxy (Quillen et al. 2009; Minchev et al. 2009).

A numerically well-studied effect of this non-axisymmetry of the Galactic potential is the radial migration of stars due to resonant scattering by transient spiral structure (SS) (Sellwood and Binney 2002, hereafter SB02; Roškar et al. 2008), which could explain the aforementioned absence of AMR in the SN. N-body simulations based on cosmological initial conditions (e.g., Heller et al. 2007) would a priori be the most natural framework in which to study radial mixing in galactic disks. However, these simulations cannot at present produce large enough thin galactic disks due to the transfer of angular momentum from the disk to the live dark matter halo. The resulting galaxies are typically thick and present large stellar velocity dispersions, so that they are closer to S0 galaxies than to MW-like ones (Sánchez-Blázquez et al. 2009). On the other hand, Roškar et al. (2008) used an N-body hydrodynamical model in which the initial conditions were designed to mimic the stage following a last major merger when the thin disk formation is supposed to start. Both SB02 and Roškar et al. (2008) compare the effects of radial migra-

[1] Université de Strasbourg, CNRS, Observatoire Astronomique, 11 rue de l'Université, 67000 Strasbourg, France; ivan.minchev@astro.unistra.fr

tion in the MW disk, for which the existence of a bar is firmly established, to a simulated galaxy lacking a central bar. Unless the effect of the bar is unimportant to the mixing process, their results would only poorly approximate the radial migration in our Galaxy. In this paper we check whether the effect of galactic bars can indeed be neglected in the context of radial migration in galactic disks, as assumed in a number of previous studies. For this purpose we study the combined effect of SS and a central bar (and more generally of multiple patterns) on the radial mixing of stars in a stellar disk.

There is observational evidence for multiple patterns in external galaxies, such as asymmetries in the spiral structure (e.g. Henry et al. 2003; Meidt et al. 2008). By expanding galaxy images in Fourier components, Elmegreen et al. (1992) noted that many galaxies exhibit hidden three-armed components and suggested that multiple spiral density waves can propagate simultaneously in galaxy discs. In addition, by means of the recently developed (Merrifield et al. 2006) Radial Tremaine-Weinberg (TWR) method, Meidt et al. (2009) analyzed the high-quality HI and CO data cubes available for four spiral galaxies. The authors found direct evidence for the presence of resonant coupling of multiple patterns, including spiral-spiral and spiral-bar components.

The results of N-body simulations provide additional motivation for studying the dynamical effects of multiple patterns. Sellwood (1985) and Sellwood and Sparke (1988) presented N-body experiments in which a bar coexists with a spiral pattern moving at a much lower angular velocity. Tagger et al. (1987) and Sygnet et al. (1988) explained this as a non-linear mode coupling between a bar and SS. Sellwood's simulations, and the theoretical explanation of Tagger et al. (1987) and Sygnet et al. (1988), were later confirmed by Masset and Tagger (1997) and Rautiainen and Salo (1999).

How do multiple patterns affect the dynamics of galactic disks? Quillen (2003) considered the dynamics of stars that are affected by perturbations from both SS and a central bar by constructing a one-dimensional Hamiltonian model for the strongest resonances in the epicyclic action-angle variables. Quillen pointed out that when two perturbers with different pattern speeds are present in the disc, the stellar dynamics can be stochastic, particularly near resonances associated with one of the patterns. Similar findings were presented more recently by Jalali (2008). All these results are not surprising since it has already been shown by Chirikov (1979) that in the case of resonance overlap the last KAM surface between the two resonances is destroyed, resulting in stochastic behavior. We therefore expect that resonance overlap could give rise to both velocity dispersion increase and radial migration.

In this paper we study the combined effect of a central bar and SS on the dynamics of a galactic disk. We concentrate on a steady-state SS in order to assess the pure effect of non-linear coupling between the two perturbers, noting that while there is strong circumstantial evidence that SS is mostly not-stationary in unbarred galaxies, the situation is less clear in barred ones (Binney and Tremaine 2008). In any case, the following model can also serve as a proxy for studying the effect of transients, and is complementary to the transient spiral mechanism developed by SB02.

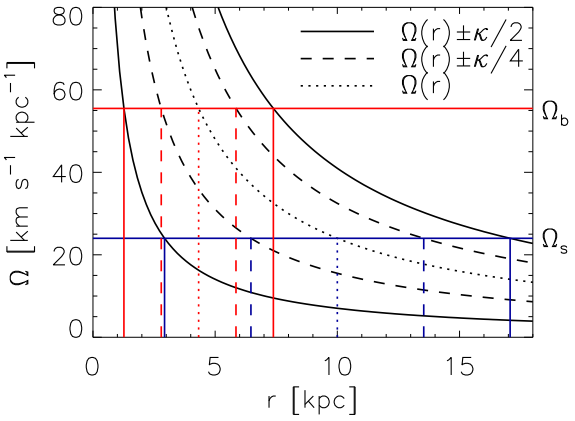

FIG. 1.— Resonances in a galactic disk for nearly circular orbits and a flat rotation curve. Corotation occurs along the dotted black curve and is given by $\Omega_{b,s} = \Omega(r)$, where $\Omega_{b,s}$ is the bar or spiral pattern speed, $\Omega(r) = v_0/r$ is the local circular frequency, and v_0 is the constant circular velocity. The 2:1 outer and inner Lindblad resonances (OLR and ILR) occur along the solid black curves, computed as $\Omega_{b,s} = \Omega(r) \pm \kappa/2$, where κ is the local radial epicyclic frequency. The outer and inner 4:1 LRs occur along the dashed black curves, given by $\Omega_{b,s} = \Omega(r) \pm \kappa/4$. The red horizontal line indicates the bar pattern speed used in this paper, $\Omega_b = 55.5$ km/s/kpc, and the blue horizontal line shows a spiral pattern speed of $\Omega_s = 24$ km/s/kpc, such as the one used in the simulations shown in Figs. 3 and 4. The vertical red and blue lines give the radial positions of each resonance for the bar and spiral structure, respectively (solid lines: 2:1; dashed lines: 4:1, dotted lines: CR).

2. RESONANCES IN GALACTIC DISKS

Galactic disks rotate differentially with nearly flat rotation curves, i.e., constant circular velocity as a function of galactic radius. In contrast, density waves, such as a central bar or SS, rotate as solid bodies. Therefore stars at different radii would experience different forcing due to the non-axisymmetric structure. Of particular interest to us are locations in the disk where the stars are in resonance with the perturber. The corotation resonance (CR), where stars move with the pattern, occur when the angular rotation rate of stars equals that of the perturber. The Lindblad resonances (LRs) occur when the frequency at which a star feels the force due to a perturber coincides with the star's epicyclic frequency, κ. As one moves inward or outward from the corotation circle, the relative frequency at which a star encounters the perturber increases. There are two values of r for which this frequency is the same as the radial epicyclic frequency. This is where the inner and outer Lindblad resonances (ILR and OLR) are located. Quantitatively, LRs occur when $\Omega_{b,s} = \Omega \pm \kappa/m$, where m is the multiplicity of the pattern. The negative sign corresponds to the ILR and the positive to the OLR. While Bertil Lindblad defined these for the case of an m=2 pattern (thus strictly speaking the ILR/OLR are the 2:1 resonances), for an m=4 pattern the ILR/OLR must be the 4:1 resonances.

Since second order resonances, i.e., 4:1 for a 2-armed spiral or bar, or 2:1 for a 4-armed spiral, can also be quite important (as will be shown later), we need to have a convenient way to refer to them. It is somewhat confusing

and unclear how the 4:1 resonances are referred to in the literature. The inner 4:1 resonance for an m=2 pattern is known as the Ultra-harmonic resonance (UHR). Some also describe the inner and outer 4:1 resonances as the IUHR and the OUHR, others as the inner and outer m=4 resonance. If the pattern multiplicity is m=4, then these become the ILR and OLR. To our knowledge, there is no terminology for the 2:1 resonances of an m=4 pattern. To simplify things, in this paper we generalize the standard notation of Lindblad resonances to allow for the existence of both 2:1 and 4:1 resonances, regardless of the multiplicity of the pattern. In other words, we will refer to the 2:1 ILR/OLR and the 4:1 ILR/OLR for both 2-armed (or bar) and 4-armed SS. Naturally, other resonances can also be described in this manner, i.e., 3:1, 5:1, 6:1 ILR/OLR, etc.

Fig. 1 illustrates the relationship between the pattern angular velocity and the radii at which resonances occur for a flat rotation curve and nearly circular orbits. Note that for two (or more) nonaxisymmetric patterns (such as bar + SS or SS + SS) moving at different angular velocities there will always exist regions in the disk where resonances overlap. As we will see later, this turns out to be crucial for the dynamics of barred galaxies.

3. NUMERICAL PROCEDURE AND CHOICE OF PARAMETERS

We follow the motion of test particles in an initially axisymmetric, 2D stellar disk with a flat rotation curve as described in detail in Minchev and Quillen (2007), in which we grow non-axisymmetric perturbations as described below. Both the initial disk stellar density, $\Sigma(r)$, and the radial velocity dispersion, $\sigma_r(r)$, decrease exponentially with radius, where we initially start with $\sigma_r(r_d) = 5$ km/s at the disk scale-length, $r_d = 3$ kpc for a MW-type galaxy. To simulate the effect of a central bar and spiral density waves we impose perturbations on the initially axisymmetric disk as done by Minchev et al. (2007) and Minchev and Quillen (2007), respectively. Both bar and spiral perturbations are grown simultaneously in 0.4 Gyr by increasing their amplitudes form 0 to the maximum values. To ensure a smooth transition to the perturbed state we use the function defined in eq. 4 from Dehnen (2000). To be able to relate parameters to the MW we work in units of the solar distance and circular velocity with corresponding values $r_0 = 8$ kpc and $v_c = 240$ km/s; this gives $\Omega_0 = 30$ km/s/kpc.

While in Minchev and Quillen (2007) and Minchev et al. (2007) we required the integration of a large number of particles in order to be able to resolve a "solar neighbourhood", here we are interested in the global behavior of a galactic disk. Therefore we have found it sufficient to integrate 10^5 particles for each simulation, distributed between an inner and outer radii, $r_{in} = 2$ and $r_{out} = 15$ kpc. We have verified that increasing the resolution to 10^7 particles does not change our results. We divide each sample into 50 radial bins and calculate the azimuthally averaged changes in angular momentum in the disk in order to estimate the induced radial migration. The time evolution of each simulation is followed for 3 Gyr. We distinguish between the SS and the bar by indicating the OLR as $\mathrm{OLR_s}$ and $\mathrm{OLR_b}$, respectively, and similarly for the case of the ILR.

3.1. *Perturbation from a central bar*

The bar strength, ϵ_b, for the case of the MW, is defined as the ratio of the forces due to the bar's quadrupole and the axisymmetric background at the Sun's radius, r_0, on the bar's major axis, $\epsilon_b = 3(A_b/v_c^2)(r_b/r_0)^3$ (Dehnen 2000), where v_c is the asymptotic circular velocity. The bar potential is then given by

$$\Phi_{\rm b} = A_{\rm b}(\epsilon_{\rm b})\cos[2(\phi-\Omega_{\rm b}t)] \times \begin{cases} \left(\frac{r_{\rm b}}{r}\right)^3 & , \ r \geq r_{\rm b} \\ 2-\left(\frac{r}{r_{\rm b}}\right)^3 & , \ r \leq r_{\rm b} \end{cases} \quad (1)$$

where $r_b = 0.8 r_{cr}$ is the bar half-length in terms of its CR, r_{cr}; in physical units $r_b = 3.44$ kpc and $r_{cr} = 4.3$ kpc.

Previous work has used as a measure of bar strength the parameter Q_T (Combes and Sanders 1981). This is the ratio of the maximum tangential force to the azimuthally averaged radial force at a given radius. From eq. 1 this definition yields $Q_T = 2A_b/v_c^2$. We examine bar amplitudes in the range $0.1 < Q_T < 0.4$ as expected from observations of various galaxies and from N-body simulations (Combes and Sanders 1981). This corresponds to $0.013 < |\epsilon_b| < 0.05$ in our units.

The bar pattern speed is chosen to be $\Omega_b = 55.5$ km/s/kpc, which for the case of our Galaxy can be written as $\Omega_b = 1.85\Omega_0$. This value is consistent with observations of external galaxies where it is found that bars are dynamically fast, i.e., $r_{cr}/r_b = 1.2 \pm 0.2$ (Aguerri et al. 2003), and is also in accordance with recent bar pattern speed determinations for the MW (Minchev et al. 2010a, 2007; Bissantz et al. 2003; Dehnen 2000).

3.2. *Perturbation from spiral structure*

The spiral potential is given by

$$\Phi_s(r,\phi,t) = \epsilon_s \cos[\alpha \ln\frac{r}{r_0} - m(\phi-\Omega_s t)], \quad (2)$$

where ϵ_s is the SS strength, related to the amplitude of the mass surface density of spirals, Σ_s, as

$$\epsilon_s \approx -2\pi G\Sigma_s r_0/(\alpha v_c^2), \quad (3)$$

as shown in Binney and Tremaine (2008). The parameter α is related to the pitch angle of the spirals, p, by $\alpha = m\cot(p)$. The azimuthal wavenumber m is an integer corresponding to the number of arms. We consider both 2-armed and 4-armed SS with $\alpha = -4$ and -8, respectively, where the negative sign corresponds to trailing spirals. Elmegreen (1998) found that grand-design spirals have arm-interarm contrasts of 1.5-6, corresponding to a fractional amplitude of $0.2 < \Sigma_s/\Sigma < 0.7$, which is in agreement with Rix and Zaritsky (1995) who estimated $0.15 < (\Sigma_s/\Sigma) < 0.6$. Since we would like to examine this range of spiral amplitudes we need to relate the relative overdensity to the relative potential.

For a maximum exponential disk the peak circular speed in the disk has the value $v_c \simeq 0.622\sqrt{GM_d/r_d}$ at $r \simeq 2.15 r_d$, where M_d is the disk mass inclosed by r_d. The surface density of the disk at radius r is $\Sigma(r) = (M_d/2\pi r_d^2)e^{-r/r_d}$. Eliminating M_d from these expressions, we find at r_0, $v_c^2 \simeq 0.39 \times 2\pi G r_d \Sigma_0 e^{r_0/r_d}$. Substituting this expression for v_c in eq. 3, the relation

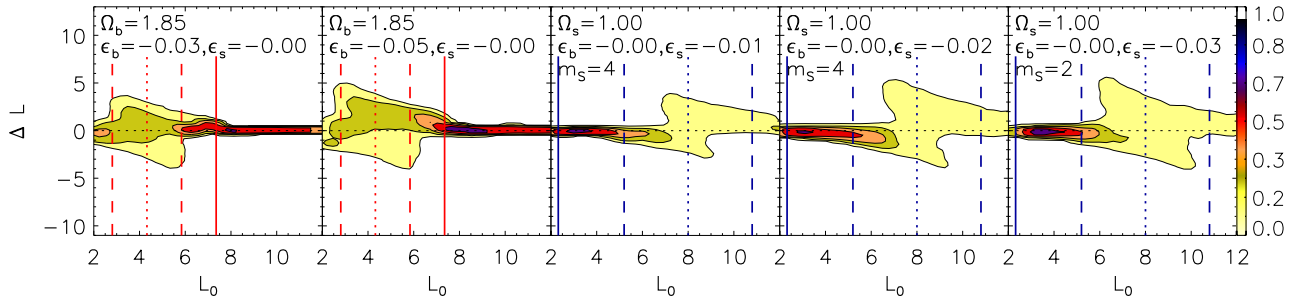

FIG. 2.— Changes in angular momentum, ΔL, as a function of the initial angular momentum, L_0. Both ΔL and L_0 are in units the circular velocity, v_c; L_0 is thus equivalent to the galactocentric distance, r, in kpc. Bar and SS amplitudes are indicated in each panel. The first two panels form left to right present simulations with a bar of an intermediate strength ($Q_T = 0.25$) and a strong one ($Q_T = 0.4$), respectively. The third and fourth panels show a 4-armed SS with relative overdensity $\Sigma_s/\Sigma_0 = 0.2, 0.35$. The rightmost panel presents a simulation with a 2-armed SS with an amplitude giving rise to $\Sigma_s/\Sigma_0 = 0.25$. The dotted lines show the corotation radii. The 2:1 and 4:1 LRs are indicated by the solid and dashed lines respectively (bar=red, spiral=blue). Note that, depending on the pattern speed, some resonances might not be present in the disk. $|\Delta L|$ increases significantly only near the corotation of each perturber.

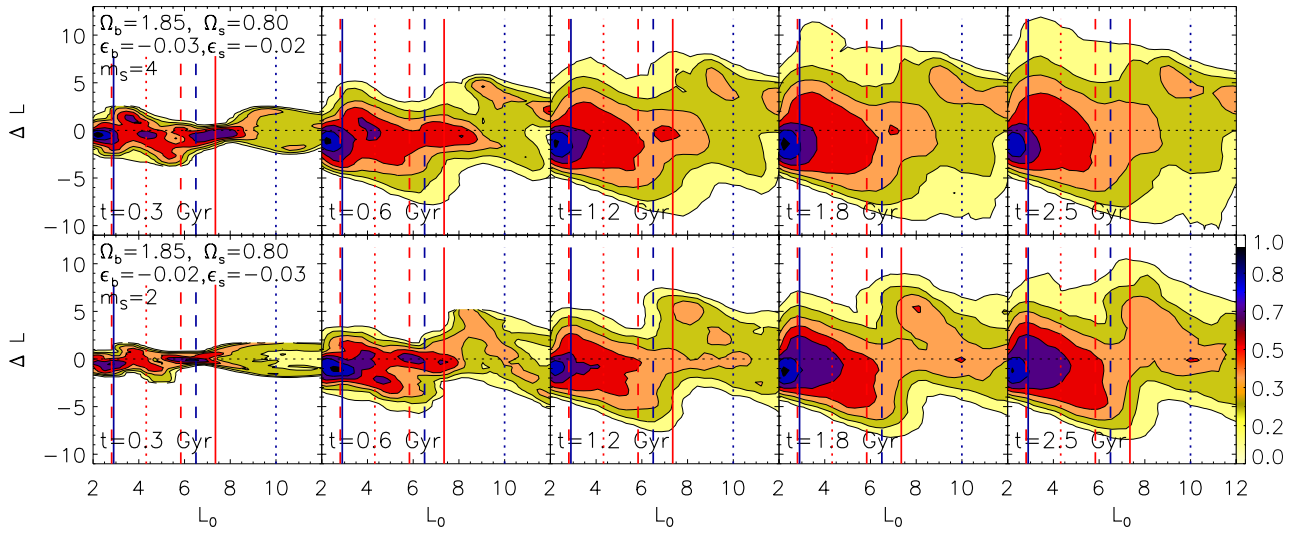

FIG. 3.— Time evolution of the changes in angular momentum, ΔL, for a stellar disk perturbed by both a central bar and SS. The top row shows a bar and a 4-armed SS of intermediate strengths: $\epsilon_b = -0.03$ ($Q_T = 0.25$) and $\epsilon_s = -0.02$ ($\Sigma_s/\Sigma_0 = 0.35$ for m=4). For the bottom row the bar and the 2-armed SS are weaker: $\epsilon_b = -0.02$ ($Q_T = 0.16$) and $\epsilon_s = -0.03$ ($\Sigma_s/\Sigma_0 = 0.25$ for m=2). The increase of ΔL with time indicates that stars are being placed on radii different than their birthplaces, i.e., radial migration takes place throughout the disk.

between the relative potential and the relative overdensity becomes

$$\epsilon_s \approx -\frac{\Sigma_s}{\Sigma_0}\frac{r_0}{r_d}\frac{e^{\frac{-r_0}{r_d}}}{0.39\alpha}. \quad (4)$$

To correct for finite disk thickness we need to decrease the right-hand side of this equation by the factor e^{-kz_0} (e.g., Vandervoort 1970), where k is the wave vector given by $k \approx \alpha/r_0$. For a MW-type galaxy we can adopt a disk scale-height of $z_0 \sim 300$ pc, resulting in $e^{-kz_0} \approx 0.86$ and 0.74 for a 2- and 4-armed SS, respectively. Using eq. 4 and accounting for finite disk thickness we estimate that the observed spiral arm amplitudes quoted above would result in potential perturbation in the range $0.007 < |\epsilon_s| < 0.031$ for a 4-armed and $0.015 < |\epsilon_s| < 0.072$ for a 2-armed SS.

4. SINGLE PERTURBATION

We now estimate the changes in angular momentum, ΔL, in a stellar disk. To do this, we divide the disk into 50 radial bins and compute $\Delta L = L_1 - L_0$, where L_0 and L_1 are the mean values of the initial (at $t = 0$) and final (at some later time, t_1) angular momenta of particles in each bin.

In Fig. 2 we show ΔL as a function of L_0 for a simulation with a single perturber. Both axes are in units of the circular velocity, v_c; L_0 is thus equivalent to the galactocentric distance, r in kpc. The bar and SS amplitudes are indicated in each panel. The first two panels from left to right present simulations with a bar of an intermediate strength ($Q_T = 0.25$) and a strong one ($Q_T = 0.4$), respectively. The third and fourth panels show a 4-armed SS with relative overdensity $\Sigma_s/\Sigma_0 = 0.2, 0.35$. The rightmost panel presents a simulation with a 2-armed SS with an amplitude giving rise to $\Sigma_s/\Sigma_0 = 0.25$. The dotted lines show the corotation radii. The 2:1 and 4:1 LRs are indicated by the solid and dashed vertical lines, respectively (bar=red, spiral=blue). Note that, depending on the pattern speed, certain resonances might not be present in the disk. The pattern speeds are given in units of the angular velocity at $r_0 = 8$ kpc, $\Omega_0 = 30$ km/s/kpc.

Significant angular momentum changes in Fig. 2 occur only near the CR of each perturber (dotted lines). No further increase in $|\Delta L|$ is apparent with time once the perturber is fully grown, which is to be expected for a time-independent perturbation. We are now interested to see what changes occur when both the bar and SS act

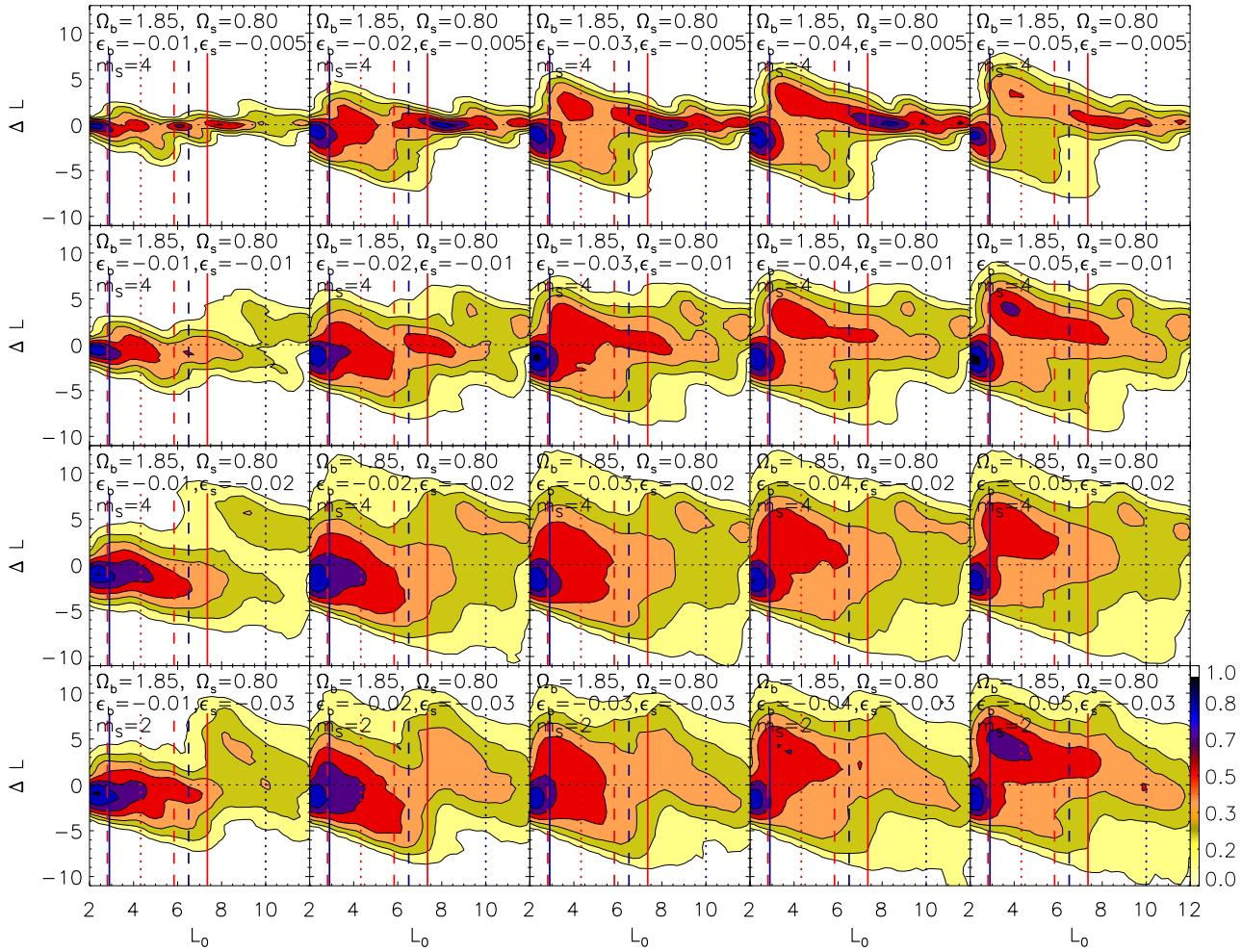

FIG. 4.— The changes in angular momentum at $t = 3$ Gyr for simulations with different perturbation strengths, while all other parameters are kept fixed. From left to right the bar strength increases as indicated in each panel. The SS strength increases from top to bottom. Note the bimodality caused by the bar's corotation and its 2:1 OLR.

together.

5. BAR + SPIRAL STRUCTURE

As shown by Minchev and Quillen (2006), when two perturbers moving at different pattern speeds are imposed on a galactic disk, an increase in the random motions of stars is expected, i.e., the disk heats. In addition, the authors found that in regions of resonance overlap stars drift radially with time from their birth radii. This suggests that such a mechanism could be responsible for radial migration in the disk. Here we quantify this idea more clearly for the case of bar + SS, by examining the effect of the simultaneous propagation of the two perturbers.

5.1. *Time evolution of* ΔL

In Fig. 3 we show the time development of the changes of angular momentum in a stellar disk perturbed by both a central bar and SS. In each row we present a different combination of bar and SS strengths, as described bellow, while all other parameters are kept fixed. As in Fig. 2, contour plots show the change in angular momentum, ΔL, as a function of the initial angular momentum L_0 (or radius, r in kpc). Panels from left to right show the temporal evolution of the system for 0.3, 0.6, 1.2, 1.8 and 2.5 Gyr. In the top row both the bar and the 4-armed SS have intermediate strengths: $\epsilon_b = -0.03$ ($Q_T = 0.25$) and $\epsilon_s = -0.02$ ($\Sigma_s/\Sigma_0 = 0.35$ for m=4). For the bottom row the bar and the 2-armed SS are weaker: $\epsilon_b = -0.02$ ($Q_T = 0.16$) and $\epsilon_s = -0.03$ ($\Sigma_s/\Sigma_0 = 0.25$ for m=2). The pattern speeds in both simulations are the same so that we can asses the effect of the different amplitudes.

Examining the first row of Fig. 3, we note that at the beginning of the simulation $|\Delta L|$ increases mainly at the CR of each perturber (dotted lines), which would be the case of linearly adding the individual effects of the bar and SS seen in Fig. 2. However, at later times large changes in angular momentum occur, suggesting that non-linear effects become important. Note that at $t = 0.6$ Gyr the effect near each CR is already stronger than that expected from each individual perturber (compare to Fig. 2). Meanwhile the area between the CRs of the bar and SS fills in with time as a result of the proximity of the 4:1 $\mathrm{ILR_s}$, the 4:1 $\mathrm{OLR_b}$ and the 2:1 $\mathrm{OLR_b}$, thus extending the effect over the entire disc. At $t = 1.8$ Gyr (fourth panel of Fig. 3), the changes in angular momentum throughout the disk are similar in amplitude to those resulting from recurrent spirals (Fig. 11 in SB02). To reach this level of mixing, however, requires less than ~ 2 Gyr compared to ~ 9 Gyr for the case of transients.

Decreasing the bar strength to $\epsilon_b = -0.02$ ($Q_T = 0.16$) (bottom row of Fig. 3) and considering a slightly weaker

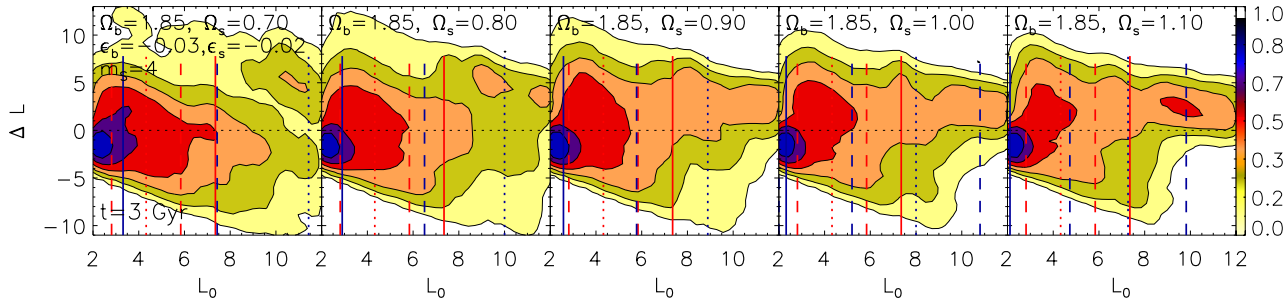

FIG. 5.— Variation of mixing with pattern speed ratio. ΔL is shown for different SS pattern speeds, Ω_s, while keeping Ω_b the same. This results in different spacing of the bar and SS resonances. From left to right the 4-armed SS moves at $\Omega_s = 0.7, 0.8, 0.9, 1.0$, and 1.1 in units of $\Omega_0 = 30$ km/s/kpc. All other simulation parameters are kept fixed: the time is $t = 3$ Gyr and the strengths of the perturbers are the same as in the top row of Fig. 3. As expected, the effect of resonance overlap on ΔL is strongest when the highest order resonances (2:1 $\mathrm{OLR_b}$ and 4:1 $\mathrm{ILR_s}$) lie closest to each other (leftmost panel, $L_0 \sim 7.5$).

2-armed SS has a weaker effect on ΔL. However, changes in ΔL are still very strong, mixing the disk in less than 3 Gyr.

At this time we can already identify two main differences between radial migration from transients and the mechanism described in this work: (1) The time-scale for disk mixing is much shorter in the case of resonance overlap and (2) resonance overlap causes a bimodal distribution in ΔL with peaks near the bar's CR and its 2:1 OLR, compared to the single peak seen in Fig. 11 and 12 in SB02. Next we explore further the effect of perturbation strengths.

5.2. *Variation with perturbation strengths*

The strong increase of $|\Delta L|$ with time when both a bar and SS perturb a stellar disk suggests that this is a nonlinear effect. We therefore expect strong variation with the strength of the perturbers. To investigate this further we now explore the effect on mixing when different combinations of ϵ_s and ϵ_b are considered. In Fig. 4 we plot the changes in angular momentum at $t = 3$ Gyr for simulations with different perturbation strengths, while all other parameters are kept fixed. From left to right the bar strength increases as indicated in each panel. The SS strength increases from top to bottom.

Observing the top, leftmost panel of Fig. 4 we see that when both perturbers are weak mixing is not very strong, although an increase in $|\Delta L|$ near the 2:1 $\mathrm{OLR_b}$ is still apparent. However, as the bar strength increases, while keeping the spiral weak, the resonance overlap in the inner disk has a surprisingly strong effect on ΔL. To realize this compare the top row of Fig. 4 to the corresponding bar strengths in Fig. 2. Similar behavior is observed in the case of a weak bar and a range of SS strengths (first column in Fig. 4). Note that here in addition to the inner disk we also see a strong effect near the spirals' CR at 10 kpc, which is well outside the 2:1 $\mathrm{OLR_b}$. A possible explanation could be the proximity of the CR of SS to the bar's 1:1 asymmetric, 1:1 symmetric resonances, or $x_1^*(2)$ unstable orbits (Dehnen 2000).

5.3. *Variation with pattern speed ratio*

In Fig. 5 we plot ΔL for different SS pattern speeds, Ω_s, while keeping Ω_b the same. This results in different spacing of the bar and SS resonances. From left to right the 4-armed SS moves at $\Omega_s = 0.7, 0.8, 0.9, 1.0$, and 1.1 in units of $\Omega_0 = 30$ km/s/kpc. All other simulation parameters are kept fixed: the time is $t = 3$ Gyr and the strengths of the perturbers are the same as in the top row of Fig. 3. As one would expect, the effect of resonance overlap on ΔL is strongest when the highest order resonances (2:1 $\mathrm{OLR_b}$ and 4:1 $\mathrm{ILR_s}$) lie very close to each other (leftmost panel, $L_0 \sim 7.5$). For all pattern speed ratios the distribution of ΔL exhibits a bimodality near the bar's CR and near its 2:1 OLR. This signature can be used to identify the mechanism described here in fully self-consistent simulations, where the disk dynamics is much more complicated and may include additional mixing due to transient spirals and small mergers.

6. IMPLICATIONS FOR THE MILKY WAY

We showed in Sec. 5 that the simultaneous propagation of a central bar and SS in a stellar disk induces radial migration. Since this is a nonlinear effect, depending on the perturbers' amplitudes, strong mixing could occur in a short period of time. Similarly to the majority of disk galaxies, the MW has been well established to be a barred galaxy, thus we expect mixing due to resonance overlap to be at work here as well. While there is no doubt that the MW has been affected by this process, it may be difficult to estimate exactly how. This migration mechanism is a strong function of the strengths of the MW bar and SS. However, it may be incorrect to use the currently observed spiral and bar amplitudes since most likely they have not been the same throughout the lifetime of the Galaxy. In fact, we expect that spirals were stronger in the past, when the disk velocity dispersion was lower, thus resulting in a more gravitationally unstable disk. In any case, given that the past history of the MW spiral and bar structure is largely unknown, we will make an estimate of how much mixing could have resulted by using the currently observed SS and bar parameters.

6.1. *Choice of bar and spiral structure parameters*

For all simulations in this paper we have used a bar pattern speed of $\Omega_b = 1.85\Omega_0$, where Ω_0 is the angular velocity at the solar circle r_0. For $r_0 = 8$ kpc and $v_c = 240$ km/s, in physical units $\Omega_b = 55.5$ km/s/kpc, consistent with recent pattern speed estimates (Minchev et al. 2010a, 2007; Bissantz et al. 2003; Dehnen 2000). Rodriguez-Fernandez and Combes (2008) estimated the strength of the MW bar to lie in the range $0.25 < Q_T < 0.4$ by fitting bar models to near infrared observations (2MASS counts). In the units used in this paper this range corresponds to $0.03 < |\epsilon_b| < 0.05$. The individual effect on ΔL of bars with amplitudes $\epsilon_b = -0.03$ and $\epsilon_b = -0.05$ can be seen in Fig. 2.

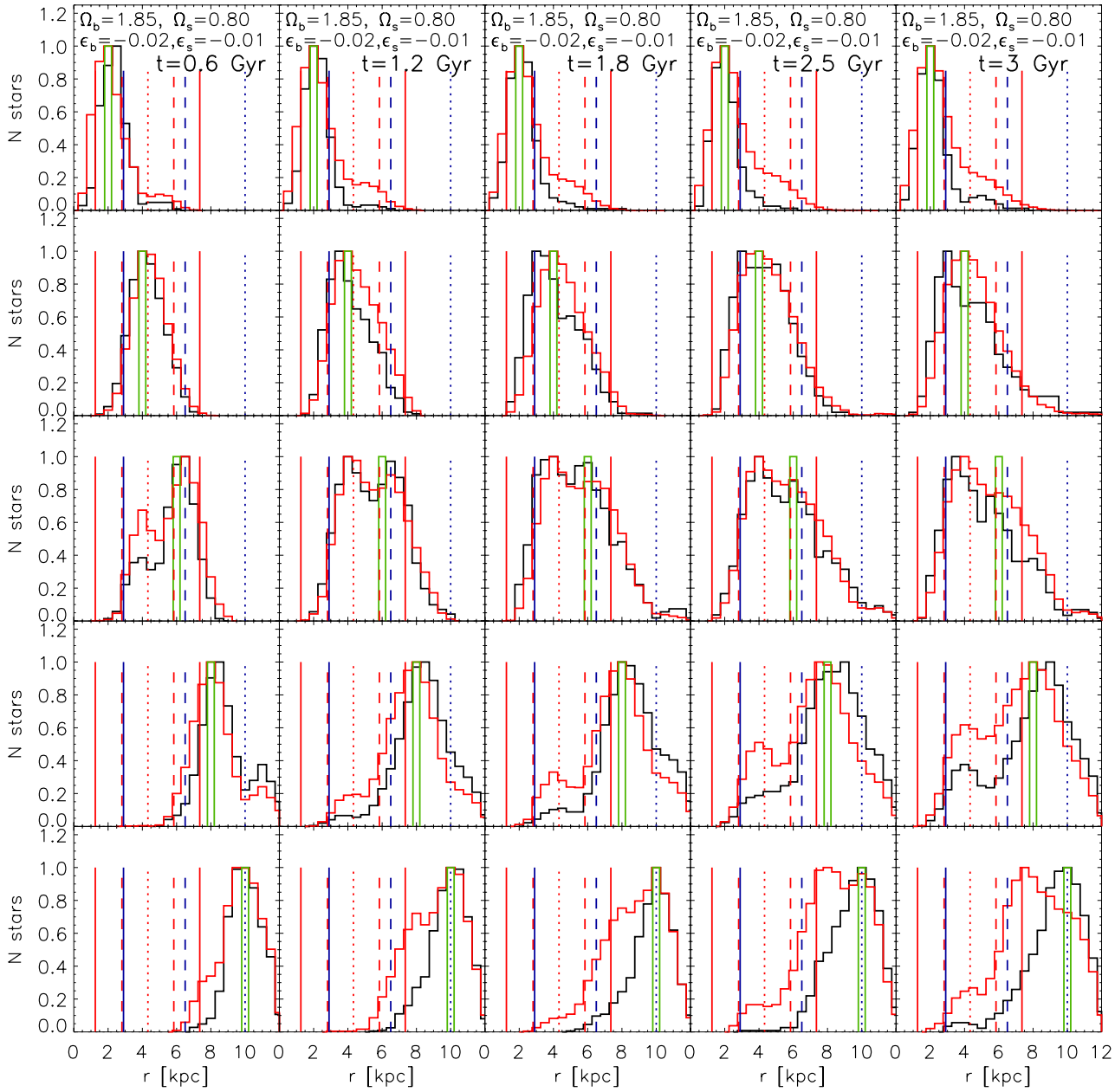

FIG. 6.— The distribution of the initial radii of stars, which have ended up in an annulus of 400 pc (in the green bin) centered at a given galactocentric distance, r. Simulation parameters are consistent with the Milky Way structure (see Sec. 6). From top to bottom different rows show the time evolution of each such annulus centered on r = 2, 4, 6, 8, and 10 kpc. The black and red histograms show stars on nearly circular orbits ($\sigma_r \sim 5$ km/s) and the total population, respectively. With this new mechanism, the solar neighborhood stars could have come from a wide range of Galactic radii, including from the outer Galaxy, and thus account for the flatness of the observed AMR. Note the different signature in the mixing of cold and hot orbits.

The MW SS parameters are much more uncertain. It has been proposed to be a superposition of 2- and 4-armed patterns moving near corotation with the Sun (Lépine et al. 2001; Torra et al. 2000). On the other hand, Martos et al. (2004) and Bissantz et al. (2003) matched the properties of the gas in the inner Galaxy with a 4-armed SS with a pattern speed of 20 km/s/kpc (or with the Sun near the 4:1 ILR). The MW SS at this stage in the Galaxy evolution appears to be quite weak compared to observations of external galaxies: Drimmel and Spergel (2001) derived $\Sigma_s/\Sigma_0 = 0.15$ for the stellar component (based on K-band observations). These authors, however, suggested that most likely this value is larger. There are also indications from the gas flow in the inner Galaxy that the MW has stronger spiral arms, where the amplitude in the mass density is larger by a factor of 1.5 than its amplitude in the near-infrared luminosity density (see Bissantz et al. 2003; Famaey and Binney 2005). Therefore, a possible range for the relative overdensity is $0.15 < \Sigma_s/\Sigma_0 < 0.23$. These values, including the correction for finite disk thickness (Sec. 3.2), correspond to a potential perturbation of $0.015 < |\epsilon_s| < 0.024$ and $0.007 < |\epsilon_s| < 0.01$ for a 2- and 4-armed SS, respectively.

From the discussion above, for parameters consistent with our Galaxy, the amount and rate of mixing due to spiral-bar resonance overlap is given by the second row of Fig. 4 for a 4-armed SS, and by the bottom row for a 2-

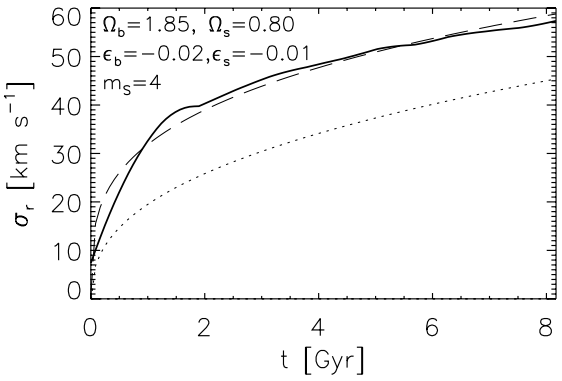

FIG. 7.— Radial velocity dispersion as a function of time at the solar radius (solid line) for the simulation in Fig. 6. The dashed line shows a power-law fit to the simulated data. The dotted line plots the observed age-velocity relation in the solar neighborhood (Holmberg et al. 2009).

armed SS (excluding the leftmost panels in both cases). Note that the strength of the 2-armed SS in Fig. 4 is slightly stronger than the estimated range.

6.2. *Mixing at different Galactic radii*

To see in greater detail how stars migrate throughout the disk we now examine the effect on mixing at different galactic radii. To be consistent with MW parameters, we use the simulation for which we presented the changes in angular momentum in Fig. 4, second row, second column. In Fig. 6 we show the distribution of birth radii (at $t = 0$) of stars which are "currently" (at the time indicated in each plot) in an annulus of 400 pc (in the green bin). Each row shows an annulus centered on a different galactic radius, r: from top to bottom $r = 2$, 4, 6, 8, and 10 kpc. To show the effect on stars placed on nearly circular orbits, the black histograms plot only stars with a cut in the eccentricity, $e < 12$. We estimate e as $e \approx \sqrt{(u^2 + 2v^2)/2}$, appropriate for a flat rotation curve (Arifyanto and Fuchs 2006), and u, v are the radial and tangential velocity components of stars with the circular velocity subtracted. The radial velocity dispersion resulting for this sample is ~ 5 km/s, insuring that stellar orbits are almost circular. The red histograms show the full sample. Stars on cold orbits, shown by the (normalized) black histograms, constitute about 10% of the total population.

Firstly, note that the distributions peak at radii near regions of resonance overlap, as expected. While in the inner disk ($r = 2$ and 4 kpc) there are strong weights at larger radii, the situation is reversed for $r \geq 6$ kpc. At the solar distance, $r = 8$ kpc (fourth row in Fig. 6), a large population of stars from the bar's CR ($r \sim 4.5$ kpc) enters the solar circle. Naturally, when the total population is considered (red histogram) more stars enter from the inner disk due to the exponential profiles of both the density and the radial velocity dispersion. Observe also the overall shift toward larger radii of the cold population compared to the total sample.

While the pattern speed of the MW SS is not well constrained, the bar is well established to have its 2:1 OLR just inside the solar circle. Since the bar's CR and OLR are both strong and roughly invariable (only small changes in the bar parameters are expected in ~ 3 Gyr), we can expect to find a bimodal distribution of ΔL with peaks at these bar resonances *regardless of the SS pattern speed*. That is exactly what is seen in Fig. 5. What if the MW spirals were transient? In that case the distribution of the changes in angular momentum can be approximated by the linear combination of a range of simulations with different SS pattern speeds (imagine adding up all panels in Fig. 5). This would again result in a bimodal distribution. Therefore, although the past history of the MW structure is not known and a large range of possible perturber strengths, pattern speeds and longevity exists, *it would be reasonable to expect to always find a bimodality in the distribution of* ΔL.

Consequently, the large fraction of stars coming from the bar's CR which enters the solar circle (fourth row of Fig. 6) may be one of the observational signatures of the spiral-bar resonance overlap mechanism. This is expected to affect the local metallicity distribution of stars. We also note that a large fraction of stars comes from the outer disk, roughly 40% of all stars for this particular pattern speed ratio. This is consistent with the metal-poor stars from the outer Galaxy scattered into the SN, as recently inferred from observational data (Haywood 2008), and a metal-rich population coming from the inner Galaxy. With this new mechanism, the SN stars could have come from a wide range of Galactic disk radii, including from the outer Galaxy, and thus can account for the flatness of the observed AMR.

On the other hand, away from the solar circle we expect to find overdensities of stars originating at the bar's 2:1 OLR. We clearly see this in the initial distribution of stars ending up in the annuli centered on $r = 2, 4, 6$ and 10 kpc (Fig. 6). This may provide another observable for identifying the currently discussed mechanism.

However, the most promising technique to put constraints on this mechanism in the MW is "chemical tagging" (Freeman and Bland-Hawthorn 2002). The idea is to use the detailed chemical abundance patterns of individual stars in our Galaxy to associate them with common ancient star-forming aggregates with similar abundance patterns. This technique will be very important to characterize the star formation and chemical histories of the MW. Chemical tagging will become possible with the HERMES survey on the Anglo-Australian Telescope (AAT; Freeman and Bland-Hawthorn 2008; Freeman et al. 2010) and the APOGEE survey at the Apache Point Observatory (Allende Prieto et al. 2008). Therefore, in the next couple of years we may be in a position to directly measure the spread of open clusters across the Galaxy as a function of age, thus providing direct constraints on the amount of mixing in the Milky Way (Bland-Hawthorn et al. 2010).

6.3. *The effect on disk heating*

Now we look at the effect on the increase of random motion of stars with time. The observed correlation between the ages and velocity dispersions of SN stars has been a subject of study since the work of Spitzer and Schwarzschild (1951, 1953) (see Minchev and Quillen 2006 for a detailed introduction). Deferent mechanisms have been proposed to explain the age-velocity relation (AVR) (or stellar disk heating), including scattering by giant molecular clouds (GMC) (e.g., Mihalas and Binney 1981) and transient spirals (e.g., Barbanis and Woltjer 1967). In Minchev and Quillen (2006) we showed that the reso-

nance overlap of multiple spiral patterns provides yet another mechanism for disk heating. We therefore expect that an overlap of bar and SS resonances would give a similar result. To check if this is indeed the case, in Fig. 7 we plot the radial velocity dispersion, σ_r, (solid line) as a function of time for the same simulation used to produce Fig. 6. The dashed line shows a power-law fit to our simulated data: $\sigma_r \sim t^{0.29}$. To compare to observations we also show the AVR in the SN (dotted line), as estimated recently from analysis of the Geneva-Copenhagen Survey data (Holmberg et al. 2009). Note that the observed AVR goes like $\sigma_r \sim t^{0.39}$. Moreover, in our simulation the disk heats $\sim 20\%$ more than observed. There could be several possibilities that could account for this discrepancy: (1) our simple model does not include a gaseous disk component nor star formation, which would naturally lower the velocity dispersion; (2) while here we considered 2D disks, a significant fraction of the heating in the galactic disk plane would be transferred to the vertical direction, where GMC serve as scattering agents (Jenkins and Binney 1990; Jenkins 1992); and (3) in this work we used constant parameters for both the MW bar and SS, but it is reasonable to expect more realistic scenarios, where throughout the lifetime of the Galaxy there could have been variations of the perturbers' amplitudes and pattern speeds, bar size, spiral pitch angle, as well as bar destruction and reformation (Bournaud and Combes 2002).

7. DISCUSSION AND CONCLUSIONS

In this work we have examined the combined effect of a central bar and spiral structure on the radial migration in galactic disks. We have found that:
(i) This new mechanism for galactic disk mixing could be up to an order of magnitude more effective than the transient spirals one (see Sec. 5.2). We note that the effect is non-linear, strongly dependent on the strengths of the perturbers. The non-linearity of the mechanism is confirmed by the fact that an increase in the amplitudes yields a much larger increase in the angular momentum changes in a simulation including *both* bar and spiral structure, compared to the case of a single perturber. In other words, the individual effects do not add up linearly. Another indication of non-linearity is that the effect increases with time only in the case of the two perturbers propagating simultaneously.
(ii) The signature of this mechanism is a bimodality in the changes of angular momentum in the disk with maxima near the bar's corotation and its outer Lindblad resonance (see Figs. 5 and 6). This is true regardless of the spiral pattern speed and can be used in identifying the spiral-bar resonance overlap migration in N-body simulations, where the disk dynamics is much more complicated.
(iii) For bar and spiral parameters consistent with Milky Way observations we find that it takes ~ 3 Gyr to achieve the mixing for which transients require 9 Gyr. In addition to radial mixing, spiral-bar coupling can account for the age-velocity relation (AVR) observed in the solar neighborhood (Fig. 7, Sec. 6.3). Note however that the estimates for the Milky Way spiral and bar strengths derived from observations *now* may simply be irrelevant for our understanding of the current state of mixing in the Galactic disk (see Sec. 6).
(iv) This mechanism could explain observations showing that strongly barred galaxies have weaker metallicity gradients than weakly barred or non-barred galaxies (e.g., Zaritsky et al. 1994; Martin and Roy 1994; Pérez et al. 2009).

The effect of resonance overlap we have described in this paper appears to be quite strong. In order for it to work, a galactic disk must contain a central bar[2]. Unlike in our test-particle simulations, where the disk responds solely to the bar potential, as seen in N-body simulations and deduced from observations, a bar is expected to always drive spiral structure (e.g., Salo et al. 2010). Thus, any barred galaxy would be affected strongly by this mechanism. As the disk heats and SS diminishes in strength, the effect on ΔL will decrease. It is therefore likely that resonance overlap migration will be most vigorous at certain periods during a galaxy lifetime.

In this work we have only considered steady-state spirals in order to assess the pure effect of the coupling between bar and spiral structure. Considering transient spirals would increase the efficiency, since the SB02 mechanism would come into play as well. Therefore, a combination of a central bar and short-lived transients is expected to be extremely efficient at mixing barred spiral galaxies.

As discussed in Sec. 6, the most promising technique to put constraints on this mechanism in the MW is "chemical tagging" (Freeman and Bland-Hawthorn 2002; Bland-Hawthorn et al. 2010) which will become possible with the forthcoming spectroscopic survey HERMES (Freeman and Bland-Hawthorn 2008; Freeman et al. 2010). More ongoing and planned large Galactic surveys, such as RAVE, SEGUE, SIM Lite, GYES, LAMOST and GAIA, can search for signatures of the mechanism (see also Minchev and Quillen 2008).

In a follow-up paper (Minchev et al. 2010b) we study the effect of resonance overlap in fully self-consistent, TreeSPH/N-body simulations including a gaseous component and star formation. The migration mechanism described in this paper can provide an explanation for the observed flatness and spread in the age-metallicity relation. Our results, however, need to be incorporated into a chemo-dynamical galactic model to properly assess the effect on the AMR, and possibly also on the formation of the thick disk, similarly to the work by Schönrich and Binney (2009).

We would like to thank Bruce Elmegreen, Ken Freeman, Arnaud Siebert, Jerry Sellwood, and James Binney for helpful communications and discussions. We also thank the anonymous referee for valuable suggestion which have greatly improved the manuscript. Support for this work was provided by ANR and RAVE.

[2] Note that resonance overlap, and thus migration, will also result from multiple spiral structure (Minchev et al. 2010b).

REFERENCES

Aguerri, J. A. L., Debattista, V. P., and Corsini, E. M.: 2003, *MNRAS* **338**, 465

Allende Prieto, C., Majewski, S. R., Schiavon, R., Cunha, K., Frinchaboy, P., Holtzman, J., Johnston, K., Shetrone, M., Skrutskie, M., Smith, V., and Wilson, J.: 2008, *Astronomische Nachrichten* **329**, 1018

Antoja, T., Figueras, F., Fernández, D., and Torra, J.: 2008, *A&A* **490**, 135

Antoja, T., Valenzuela, O., Pichardo, B., Moreno, E., Figueras, F., and Fernández, D.: 2009, *ApJ* **700**, L78

Arifyanto, M. I. and Fuchs, B.: 2006, *A&A* **449**, 533

Barbanis, B. and Woltjer, L.: 1967, *ApJ* **150**, 461

Binney, J. and Tremaine, S.: 2008, *Galactic Dynamics: Second Edition*, Princeton University Press

Bissantz, N., Englmaier, P., and Gerhard, O.: 2003, *MNRAS* **340**, 949

Bland-Hawthorn, J., Krumholz, M. R., and Freeman, K.: 2010, *ApJ* **713**, 166

Bournaud, F. and Combes, F.: 2002, *A&A* **392**, 83

Chirikov, B. V.: 1979, *Phys. Rep.* **52**, 263

Combes, F. and Sanders, R. H.: 1981, *A&A* **96**, 164

Daflon, S. and Cunha, K.: 2004, *ApJ* **617**, 1115

Dehnen, W.: 1998, *AJ* **115**, 2384

Dehnen, W.: 2000, *AJ* **119**, 800

Drimmel, R. and Spergel, D. N.: 2001, *ApJ* **556**, 181

Edvardsson, B., Andersen, J., Gustafsson, B., Lambert, D. L., Nissen, P. E., and Tomkin, J.: 1993, *A&A* **275**, 101

Elmegreen, B. G., Elmegreen, D. M., and Montenegro, L.: 1992, *ApJS* **79**, 37

Elmegreen, D. M.: 1998, *Galaxies and galactic structure*

Famaey, B. and Binney, J.: 2005, *MNRAS* **363**, 603

Famaey, B., Jorissen, A., Luri, X., Mayor, M., Udry, S., Dejonghe, H., and Turon, C.: 2005, *A&A* **430**, 165

Freeman, K. and Bland-Hawthorn, J.: 2002, *ARA&A* **40**, 487

Freeman, K. and Bland-Hawthorn, J.: 2008, in T. Kodama, T. Yamada, & K. Aoki (ed.), *Astronomical Society of the Pacific Conference Series*, Vol. 399 of *Astronomical Society of the Pacific Conference Series*, pp 439–+

Freeman, K., Bland-Hawthorn, J., and Barden, S.: 2010, AAO Newsletter (February), in press

Haywood, M.: 2008, *MNRAS* **388**, 1175

Heller, C. H., Shlosman, I., and Athanassoula, E.: 2007, *ApJ* **671**, 226

Henry, A. L., Quillen, A. C., and Gutermuth, R.: 2003, *AJ* **126**, 2831

Holmberg, J., Nordström, B., and Andersen, J.: 2009, *A&A* **501**, 941

Jalali, M. A.: 2008, *ApJ* **689**, 134

Jenkins, A.: 1992, *MNRAS* **257**, 620

Jenkins, A. and Binney, J.: 1990, *MNRAS* **245**, 305

Lépine, J. R. D., Mishurov, Y. N., and Dedikov, S. Y.: 2001, *ApJ* **546**, 234

Martin, P. and Roy, J.: 1994, *ApJ* **424**, 599

Martos, M., Hernandez, X., Yáñez, M., Moreno, E., and Pichardo, B.: 2004, *MNRAS* **350**, L47

Masset, F. and Tagger, M.: 1997, *A&A* **322**, 442

Meidt, S. E., Rand, R. J., and Merrifield, M. R.: 2009, *ApJ* **702**, 277

Meidt, S. E., Rand, R. J., Merrifield, M. R., Shetty, R., and Vogel, S. N.: 2008, *ApJ* **688**, 224

Merrifield, M. R., Rand, R. J., and Meidt, S. E.: 2006, *MNRAS* **366**, L17

Mihalas, D. and Binney, J.: 1981, *Galactic astronomy: Structure and kinematics /2nd edition/*

Minchev, I., Boily, C., Siebert, A., and Bienayme, O.: 2010a, *MNRAS accepted, arXiv:0909.3516*

Minchev, I., Famaey, B., Combes, F., Di Matteo, P., Mouhcine, M., and Wozniak, H.: 2010b, *arXiv:1006.0484*

Minchev, I., Nordhaus, J., and Quillen, A. C.: 2007, *ApJ* **664**, L31

Minchev, I. and Quillen, A. C.: 2006, *MNRAS* **368**, 623

Minchev, I. and Quillen, A. C.: 2007, *MNRAS* **377**, 1163

Minchev, I. and Quillen, A. C.: 2008, *MNRAS* **386**, 1579

Minchev, I., Quillen, A. C., Williams, M., Freeman, K. C., Nordhaus, J., Siebert, A., and Bienaymé, O.: 2009, *MNRAS* **396**, L56

Nordström, B., Mayor, M., Andersen, J., Holmberg, J., Pont, F., Jørgensen, B. R., Olsen, E. H., Udry, S., and Mowlavi, N.: 2004, *A&A* **418**, 989

Pérez, I., Sánchez-Blázquez, P., and Zurita, A.: 2009, *A&A* **495**, 775

Quillen, A. C.: 2003, *AJ* **125**, 785

Quillen, A. C. and Minchev, I.: 2005, *AJ* **130**, 576

Quillen, A. C., Minchev, I., Bland-Hawthorn, J., and Haywood, M.: 2009, *MNRAS* **397**, 1599

Rautiainen, P. and Salo, H.: 1999, *A&A* **348**, 737

Rix, H. and Zaritsky, D.: 1995, *ApJ* **447**, 82

Rodriguez-Fernandez, N. J. and Combes, F.: 2008, *A&A* **489**, 115

Roškar, R., Debattista, V. P., Quinn, T. R., Stinson, G. S., and Wadsley, J.: 2008, *ApJ* **684**, L79

Salo, H., Laurikainen, E., Buta, R., and Knapen, J. H.: 2010, *ApJ* **715**, L56

Sánchez-Blázquez, P., Courty, S., Gibson, B. K., and Brook, C. B.: 2009, *MNRAS* **398**, 591

Schönrich, R. and Binney, J.: 2009, *MNRAS* **396**, 203

Sellwood, J. A.: 1985, *MNRAS* **217**, 127

Sellwood, J. A. and Binney, J. J.: 2002, *MNRAS* **336**, 785

Sellwood, J. A. and Sparke, L. S.: 1988, *MNRAS* **231**, 25P

Spitzer, Jr., L. and Schwarzschild, M.: 1951, *ApJ* **114**, 385

Spitzer, Jr., L. and Schwarzschild, M.: 1953, *ApJ* **118**, 106

Sygnet, J. F., Tagger, M., Athanassoula, E., and Pellat, R.: 1988, *MNRAS* **232**, 733

Tagger, M., Sygnet, J. F., Athanassoula, E., and Pellat, R.: 1987, *ApJ* **318**, L43

Torra, J., Fernández, D., Figueras, F., and Comerón, F.: 2000, *Ap&SS* **272**, 109

Vandervoort, P. O.: 1970, *ApJ* **161**, 87

Wilson, T. L. and Rood, R.: 1994, *ARA&A* **32**, 191

Xu, Y., Reid, M. J., Zheng, X. W., and Menten, K. M.: 2006, *Science* **311**, 54

Zaritsky, D., Kennicutt, Jr., R. C., and Huchra, J. P.: 1994, *ApJ* **420**, 87